THE JOURNAL OF BIOLOGICAL CHEMISTRY
Vol. 279, No. 32, Issue of August 6, pp. 33323–33335, 2004

Printed in U.S.A.

Binding Specificity of Sea Anemone Toxins to Na_v 1.1–1.6 Sodium Channels

UNEXPECTED CONTRIBUTIONS FROM DIFFERENCES IN THE IV/S3-S4 OUTER LOOP*

Received for publication, April 20, 2004, and in revised form, May 26, 2004
Published, JBC Papers in Press, May 28, 2004, DOI 10.1074/jbc.M404344200

Joacir Stolarz Oliveira‡§¶, Elisa Redaelli‖¶, André J. Zaharenko‡§, Rita Restano Cassulini‖, Katsuhiro Konno§, Daniel C. Pimenta§, José C. Freitas‡§, Jeffrey J. Clare, and Enzo Wanke‖‡‡**

*From the ‖Dipartimento di Biotecnologie e Bioscienze, Università di Milano-Bicocca, Piazza della Scienza, 2, Milan 20126, Italy, ‡Departamento de Fisiologia do Instituto de Biociências, Universidade de São Paulo, Rua do Matão 101, Travessa 14, 05508-900 São Paulo, Brazil, §Centro de Toxinologia Aplicada CAT/CEPID-FAPESP, Instituto Butantan, Avenue Vital Brasil, 1500, 05503-900 São Paulo, Brazil, and **Gene Expression and Protein Biochemistry, GlaxoSmithKline, Medicines Research Center, Gunnels Wood Road, Stevenage, Hertfordshire SG1 2NY, United Kingdom*

Sea anemones are an important source of various biologically active peptides, and it is known that ATX-II from *Anemonia sulcata* slows sodium current inactivation. Using six different sodium channel genes (from Na_v1.1 to Na_v1.6), we investigated the differential selectivity of the toxins AFT-II (purified from *Anthopleura fuscoviridis*) and Bc-III (purified from *Bunodosoma caissarum*) and compared their effects with those recorded in the presence of ATX-II. Interestingly, ATX-II and AFT-II differ by only one amino acid (L36A) and Bc-III has 70% similarity. The three toxins induced a low voltage-activated persistent component primarily in the Na_v1.3 and Na_v1.6 channels. An analysis showed that the 18 dose-response curves only partially fit the hypothesized binding of Lys-37 (sea anemone toxin Anthopleurin B) to the Asp (or Glu) residue of the extracellular IV/S3-S4 loop in cardiac (or nervous) Na^+ channels, thus suggesting the substantial contribution of some nearby amino acids that are different in the various channels. As these channels are atypically expressed in mammalian tissues, the data not only suggest that the toxicity is highly dependent on the channel type but also that these toxins and their various physiological effects should be considered prototype models for the design of new and specific pharmacological tools.

As voltage-gated Na^+ channels are responsible for the conduction of electrical impulses in most excitable tissues in the majority of animals (with the exception of nematodes), they have become important targets for the toxins of venomous animals from sea anemones to mollusks, scorpions, spiders, and even fishes. The peptides found in these venoms constitute various tools by means of which physiologists and pharmacologists can study the structure/function relationships of channel proteins in detail (1).

The α-subunits of voltage-gated Na^+ channels (Na_v1.x) have been divided into at least nine subtypes based on their tetrodotoxin binding, tissue expression, and amino acid sequences (2). Interestingly, the genes for four isoforms (Na_v1.1,[1] Na_v1.2, Na_v1.3, and Na_v1.7) are located in human chromosome 2. Other genes (Na_v1.5, Na_v1.8, and Na_v1.9) are located on chromosome 3, and Na_v1.4 and Na_v1.6 are located on chromosomes 17 and 12, respectively (2).

During their evolution, different animals have developed a set of cysteine-rich peptides capable of binding different extracellular sites of the channel protein. A fundamental question concerning the mechanism of action of these toxins is whether they act at a common receptor site in Na^+ channels when exerting their different pharmacological effects or at distinct receptor sites in different Na_v channels subtypes whose particular properties lead to these pharmacological differences (1).

The aim of this study was to investigate the putative ability of some peptides to distinguish the different Na^+ channels subtypes (from Na_v1.1 to Na_v1.6) either by differing biophysical effects or by differing potency or both. We used three sea anemone toxins, which have a range of sequence similarity, that were purified from different animals: the well known *Anemonia sulcata* ATX-II peptide (3); the *Anthopleura fuscoviridis* AFT-II peptide (4); and the *Bunodosoma caissarum* Bc-III peptide (5). They are all 47–48-aa-long and have three disulfide bonds; however, interestingly, two peptides (ATX-II and AFT-II) differ by only one amino acid, whereas Bc-III has only a 70% identity. To the best of our knowledge, this is the first report of the characterization of sea anemone toxins against such a wide range of sodium channel subtypes.

MATERIALS AND METHODS

Bc-III Purification

Animal and Venom Collection—30 specimens of *B. caissarum* were collected during periods of low tide-free diving at different rocky shores of the São Sebastião Channel on the northern coast of São Paulo, Brazil. The animals were transported live and starved in an aquarium for 24 h to eliminate any gastrovascular contents. The venom was obtained directly by means of nematocyst discharge as described by Malpezzi *et al.* (5). The protein content was estimated by means of absorbance at 280 nm and the BCA method (Pierce) following the manufacturer's instructions.

* This study was supported by grants from the Italian Ministero dell'Università e della Ricerca Scientifica e Tecnologica (MIUR-COFIN 2001055320, MIUR-FIRB-RBNE01XMP4-002, and MIUR-FISR 0300179) (to E. W.), FAPESP grants (to A. J. Z. and J. C. F.), and a CAPES grant (to J. S. O). The costs of publication of this article were defrayed in part by the payment of page charges. This article must therefore be hereby marked "*advertisement*" in accordance with 18 U.S.C. Section 1734 solely to indicate this fact.

¶ Both authors contributed equally to this work.
‡‡ To whom correspondence should be addressed. Tel.: 390264483303; E-mail: enzo.wanke@unimib.it.

[1] The abbreviations used are: Na_v1.1, α-subunits of voltage-gated Na^+ channel isoform; ApB, Anthopleurin B.

Purification Procedures—The *B. caissarum* venom was fractionated in a Sephadex G-50 column (1.9 × 131 cm, Amersham Biosciences), equilibrated, and eluted with 0.1 M ammonium acetate (pH 7.0) at room temperature (5, 6). At each run, ~1.0–2.0 g of the lyophilized material (corresponding to ~200 mg of protein content) was dissolved in 15 ml of the same buffer and injected into the column. Fractions of 10 ml volume were collected using an automatic Fraction Collector Frac-100 (Amersham Biosciences), absorbance (280 nm) was monitored by a Spectra/Chrom Flow Thru UV monitor/controller (Spectrum), and the elution profile was recorded by a Spectra/Chrom 1 channel recorder (Spectrum). Each corresponding peak was pooled and lyophilized, and the neurotoxic fraction (peak IIIa) was further purified by reverse-phase high performance liquid chromatography. After being diluted in Milli-Q water (Millipore Inc.), the same fraction was injected into an Ultrasphere octadecylsilyl column (4.6 × 150 mm, 5 μm, Beckman Inc.) coupled to a Shimadzu high performance liquid chromatography purification system consisting of a UV-visible detector (SPD-10A VP), pumps (LC-10AD VP), and a system controller (SCL-10A VP, Shimadzu Corp., Tokyo, Japan). The peaks were obtained using a linear gradient of 5–50% buffer B containing 90% CH_3CN and 10% buffer A (0.1% trifluoroacetic acid in H_2O) over 25 min. The flow rate was 1.0 ml/min, and UV was monitored at 214 nm. Pure Bc-III was obtained by means of repurification using the same column under 28% buffer B and at a higher flow rate (1.2 ml/min). The Bc-III and AFT-II mass spectra were obtained using a Q-TOF mass spectrometer (Micromass) in Qq-orthogonal time-of-flight configuration. An Ettan matrix-assisted laser desorption ionization time-of-flight/Pro mass spectrometer (Amersham Biosciences) was also used with α-cyano-4-hydroxycinnamic acid as the matrix. Both machines were operated in positive mode. The amino acid sequence of Bc-III was confirmed by means of N-terminal determination using automatic Edman degradation and a PPSQ/230 gas-phase sequencer (Shimadzu Corp.). A search for peptide homology/similarity and multiple sequence alignment was performed using the BLAST (www.ncbi.nlm.nih.gov) and Swiss-Prot databases (www.expasy.ch/sprot/sprot-top.html). The accession numbers are P01528 for ATX-II, P10454 for AFT-II, and A37435 for Bc-III.

ATX-II was obtained from Sigma, and AFT-II was a kind gift from Dr. Koji Muramoto (Department of Biological Science at Tohoku University) (4). All of the chemicals were of the highest purity available, and double-distilled water was used throughout.

LD_{50} Determination—The LD_{50} of Bc-III was determined intraperitoneally using white BALB/C mice (*Mus musculus*) according to Meier and Theakston (7).

Electrophysiology

Cell Culture—Human embryonic kidney 293 cell lines stably expressing human $Na_v1.1$, 1.2, 1.3, 1.5, and 1.6 (cultured in Dulbecco's modified Eagle's medium supplemented with 10% fetal bovine serum) were obtained by transfection with the corresponding pCIN5 expression vector (8) and selection of G418-resistant clones. pCIN5-hNa_V1.3 and 1.6 were generated as described previously (9, 10). pCIN5-hNa_V1.2 was generated from the hNa_V1.2 cDNA clone described in Xie *et al.* (11), pCIN5-hNa_V1.1 was generated using a human $Na_V1.1$ cDNA assembled from partial clones isolated from human adult cerebellum and medulla cDNA libraries, and pCIN5-hNa_V1.5 was generated using a human $Na_V1.5$ cDNA assembled from partial clones isolated from a cDNA library made from human heart.[2] $Na_v1.4$-expressing cells were obtained after transient transfection of a plasmid containing the hNa_v1.4 construct (a kind gift from Prof. Diana Conti-Camerino, University of Bari).

Solutions and Drugs—The standard extracellular solution contained (in mM) 130 NaCl, 5 KCl, 2 $CaCl_2$, 2 $MgCl_2$, 10 HEPES-NaOH, and 5 D-glucose, pH 7.4. The standard pipette solution contained (in mM) 130 K^+-aspartate, 10 NaCl, 2 $MgCl_2$, 10 EGTA-KOH, and 10 HEPES-KOH, pH 7.3. Known quantities of the toxins were dissolved in the extracellular solution immediately before the experiments. When contaminating potassium currents were seen, tetrodotoxin (Sigma) was used at 100 nM (on $Na_v1.1$, 1.2, 1.3, 1.4, and 1.6 currents) and the resulting traces were subtracted from control traces to obtain the tetrodotoxin-sensitive currents. The $Na_v1.5$ clone, which has a tetrodotoxin ID_{50} much higher than 100 nM, never showed significant potassium currents at the test potentials. The extracellular solutions were delivered through a 9-hole (0.6-mm) remote-controlled linear positioner with an average response time of 2–3 s that was placed near the cell under study.

Patch Clamp Recordings and Data Analysis—The currents were recorded at room temperature by means of the MultiClamp 700A (Axon Instruments) as described previously (12) with a pipette resistance of ~1.5–2.2 megaohms. Cell capacitance and series resistance errors were carefully compensated for (85–90%) before each voltage clamp protocol was run to reduce the voltage errors to <5% of the protocol pulse. The P/N leak procedure was routinely used. Voltage-dependent steady-state inactivation was determined by means of a double-pulse protocol in which a conditioning pulse was applied from a holding potential of −80 mV to a range of potentials from −110 (or −130) to −10 (or −30) in 10- or 15-mV increments for 450 ms immediately followed by a test pulse to −10 (or −20) mV. The peak current amplitudes during the tests were normalized to the amplitude of the first pulse and plotted against the potential of the conditioning pulse. The data were fitted using two exponential terms and a constant value beginning at the current peak. When necessary, the time constant of the fast inactivating term was fixed to the average fast time constant obtained in control curves. Recovery from inactivation was determined using a three-pulse protocol, which began with conditioning depolarization from a holding potential of −120 to −10 (or −20) mV for 60 (or 100) ms that inactivated >95% of the channels. This was followed by an increasing recovery time interval at −80 mV and a test depolarization to −10 (or −20) mV. The time intervals in successive episodes were 2, 5, 10, 20, and 50 ms (see details in the figure legends). pClamp 8.2 (Axon Instruments) and Origin 7 (Microcal Inc.) software were routinely used during data acquisition and analysis.

RESULTS

Bc-III and AFT-II Purification, Amino Acid Sequence, and LD_{50}—Gel-filtration chromatography of *B. caissarum* venom yielded six main peaks (I–VI). Peak IIIa (Fig. 1*A*) had the greatest neurotoxicity and was further purified by reverse-phase high performance liquid chromatography steps, leading to the pure toxin Bc-III (Fig. 1*B*). Mass spectrometry analysis showed that the molecular mass of Bc-III was 4.976 atomic mass units (4.973) (5) and that the determination of 25 N-terminal amino acid residues (GVACRCDSDGPTSRGNTLTGTLWLT) by automated Edman degradation confirmed the identity of the major toxin Bc-III (Table I) reported by Malpezzi *et al.* (5). The high purity of AFT-II was determined by mass spectrometry, and its molecular mass was also confirmed (4.941 atomic mass units). The intraperitoneal LD_{50} of Bc-III in mice was 600 μg/kg, very similar to that reported for AFT-II (450 μg/kg) (4).

Basic Properties of Biophysical Effects of ATX-II on $Na_v1.5$ and Data Analysis—As explained under "Materials and Methods," all of the experiments were performed at fixed drug concentrations using the currents elicited before and during drug perfusion (for 25–40 s) at successively increasing concentrations. Recovery was always checked after the experiment.

It is well known that the main action of sea anemone neurotoxins is to slow the inactivation process. Therefore, we mainly used protocols (double pulse, see Fig. 2*A*, *inset*) capable of deriving these properties and compared traces at the same test potential under the control conditions and during toxin perfusion. The action of ATX-II on the $Na_v1.5$ channel was the starting point used to establish the protocols for recording the data and analyzing the results. Observation of the action of increasing toxin concentrations clearly showed in first approximation that the drug is in equilibrium at a fixed concentration with a fraction of the total number of channels on each cell. We checked this result several times and consequently analyzed the data on the assumption that each Na^+ current trace is the sum of two exponential decaying components and a steady-state component. Under control conditions, the amplitude of the fast component was generally large and the other two components were normally very low or negligible. During toxin action, there was a large

[2] J. J. Clare, unpublished data.

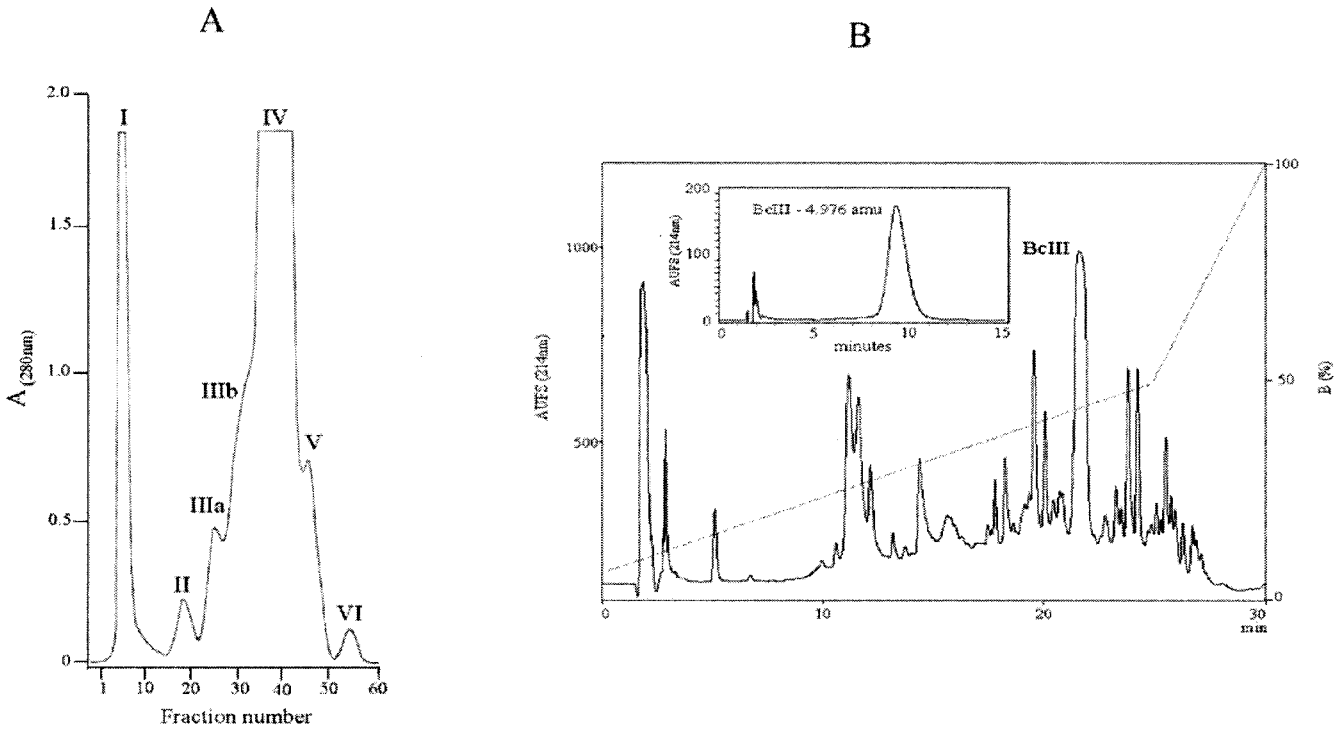

FIG. 1. **Purification procedure.** *A*, gel filtration chromatography of *B. caissarum* venom. At each run, 1.0–2.0 g of lyophilized venom (~200 mg of protein content) was injected into a Sephadex G-50 column and eluted with 0.1 M ammonium acetate buffer (pH 7.0) with 10-ml fractions being collected during UV (280 nm) monitoring. *B*, chromatographic reverse-phase high performance liquid chromatography separation of the Bc-III toxin from *B. caissarum*. Fraction IIIa was injected in an octadecysilyl column (4.6 × 150 mm) and eluted using a linear gradient of 5–50% buffer B (1.0 ml/min and 214 nm) as described under "Materials and Methods." Pure Bc-III toxin was obtained by means of a further step of purification under 28% fixed concentration of buffer B (*inset*).

TABLE I

Amino acid sequence of ATX-II, Bc-III, and AFT-II compared with other similar sea anemone toxins (the numbers refer to ATX-II)

Identical amino acids have a white background. Homologous amino acids have gray background. Different amino acids have black background. I (%) indicates the percentage of identity in comparison with ATX-II. The dashes represent gaps, and the connecting lines indicate the disulfide bonds.

	1	10	20	30	40	47	I (%)
ATX-II	- G V P C L C D S D G P S V R G N T L S G I I W L - - A G C P S G W H N C K K H G P T I G W C C K Q						100
AFT-II	G G V P C L C D S D G P S V R G N T L S G I I W L - - A G C P S G W H N C K A H G P T I G W C C K Q						97
AP-C	- G V P C L C D S D G P S V R G N T L S G I L W L - - A G C P S G W H N C K A H G P T I G W C C K Q						95
AP-B	- G V P C L C D S D G P R P R G N T L S G I L W F Y P S G C P S G W H N C K A H G P N I G W C C K K						79
BcIII	- G V A C R C D S D G P T S R G N T L T G T L W L T - G G C P S G W H N C R G S G P F I G Y C C K K						68
BgII	- G A S C R C D S D G P T S R G N T L T G T L W L I - G R C P S G W H N C R G S G P F I G Y C C K Q						68
BgIII	- G A S C R C D S D G P T S R G D T L T G T L W L I - G R C P S G W H N C R G S G P F I G Y C C K Q						66
ATX-I	- G A A C L C K S D G P N T R G N S M S G T I W V F - - G C P S G W N N C E G R - A I I G Y C C K Q						61

increase in the slow component and, in some cases (depending on the toxin type), an additional increase in a persistent component. We also systematically observed that the quality of fitting of the toxin-induced currents was not different whether we used a free or fixed (control value) fast time constant. This strongly suggests that the currents recorded in the presence of the toxin were always the sum of two types of currents: those deriving from toxin-bound channels (modified) and those deriving from toxin-free channels (not modified and thus equivalent to control channels). This is shown in Fig. 2, *A–C*, at 0, 10, and 200 nM [ATX-II]. In Fig. 2*D*, a single trace (*continuous line*) elicited at −20 mV in the presence of 5 nM toxin was dissected into a fast (○) and slow component (△). The relative increase and decrease in these components is plotted in Fig. 2*E* for different concentrations ($n = 4$), which shows that the contribution of bound and unbound channels consistently changes in relation to the toxin concentration.

Following this finding, we investigated the recovery from inactivation at −80 mV (see protocol below Fig. 2*F*) at the maximal concentration by superimposing the traces of the control (*line*), toxin (*line*), and toxin control (*open circle*). It can be seen that there was hardly any recovery of the slow component during times of the order of the time constants of recovery from inactivation in the control traces.

The normalized voltage dependence of the slow component amplitudes at the various concentrations was plotted as a function of the preconditioning level and compared with the

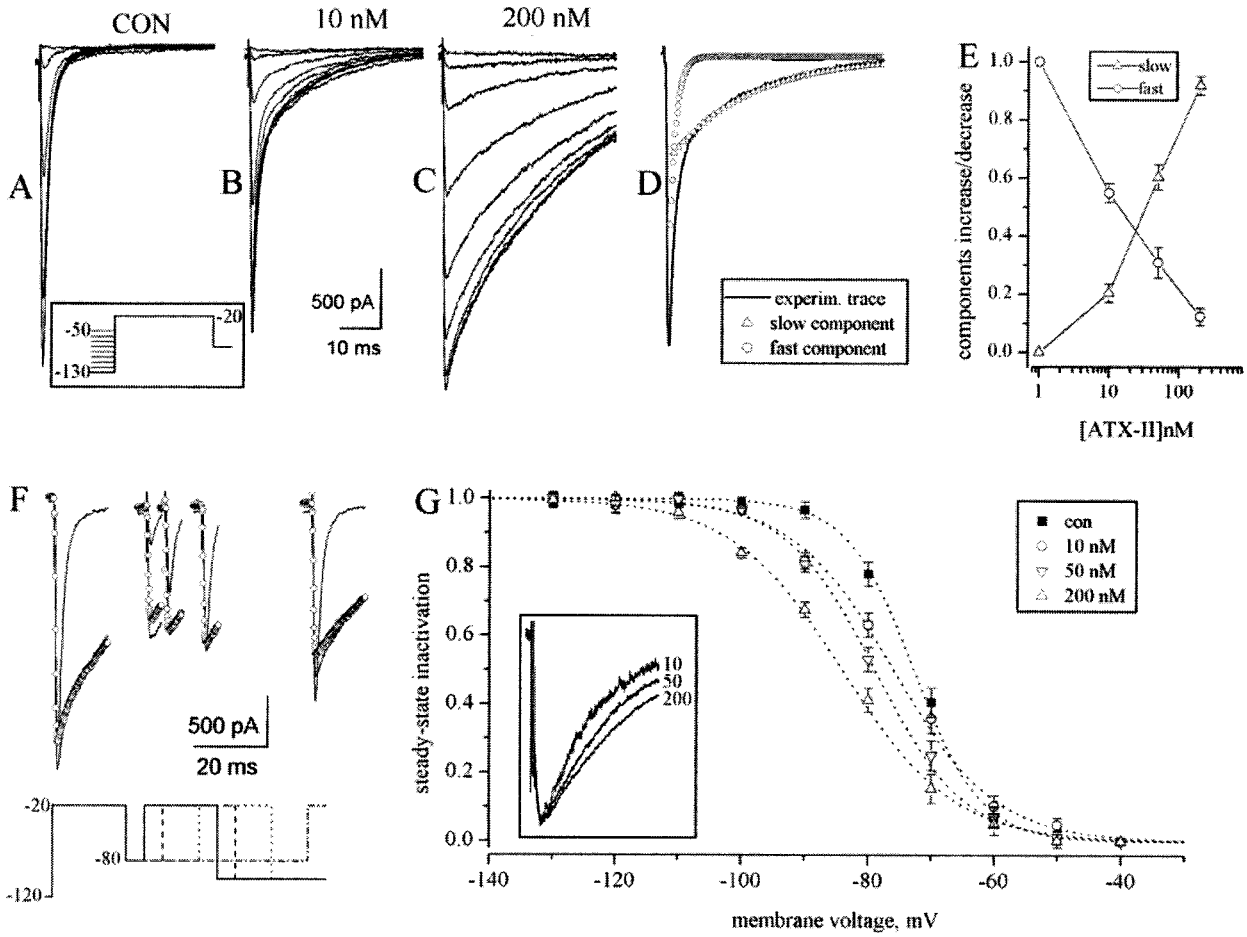

FIG. 2. **Effects of ATX-II on $Na_v1.5$ channels.** *A–C*, superimposed recordings of inward currents in control (*A*) and during the application of 10 nM (*B*) and 200 nM ATX-II (*C*) to single cells (voltage command protocol shown in the *inset* to Fig. 1*B*, one single cell). The *inset* to *panel A* shows the superimposed inward currents elicited from −130 mV at the indicated ATX-II concentrations. *D*, the fitting procedure for the first *panel B* episode (from −130 to −20 mV) showing the two exponential decaying components and the control trace. *F*, superimposed recordings of the currents elicited using the protocol shown below for studying the recovery from inactivation at −80 mV for 5, 10, 20, and 50 ms under control conditions (*continuous line*) with 200 nM ATX-II (*continuous line*) and toxin-control (*open circle*). *G*, steady-state inactivation in control and during the application of 10, 50, and 200 nM ATX-II (see different symbols) (mean values ± S.E., $n = 4$). At the three ATX-II concentrations, the plotted values are the amplitudes of the slow inactivation component deduced from the best fits of the traces (see "Material and Methods"). The continuous curves are Boltzmann relationships with the following $V_{½}$ and slope values: control (*CON*), −72.7 ± 1.1 and 5.34 ± 0.25; *10 nM*, −76.1 ± 1.3 and 8.2 ± 0.35; *50 nM*, −79.1 ± 0.91 and 7.2 ± 0.35; and *200 nM*, −84.4 ± 2.1 and 8.87 ± 0.55. *Inset*, superimposed and scaled traces of the recordings derived from elaborating the difference between the ATX-II and the control traces (see "Materials and Methods"). Note that the time constant of slow inactivation increases with the ATX-II concentration.

classical steady-state inactivation as shown in Fig. 2*G*. It can be observed that the toxin induced a net leftward shift of the slow component in comparison with the control inactivation. Moreover, comparison of the slow component at increasing concentrations indicates an increased time constant (from 14.5 to 33.2 ms, see Fig. 2*G*, *inset*), although this observation was not investigated further.

The Effect of AFT-II and Bc-III on $Na_v1.5$—The effects of the toxins AFT-II and Bc-III on $Na_v1.5$ are shown in Fig. 3. In the six panels, the data are divided along the two columns for AFT-II ($n = 4$) and Bc-III ($n = 4$). The *top row* (Fig. 3, *A* and *B*) shows the control data (*line*) with the data observed at various concentrations (different symbols of the superimposed traces in a representative cell). The *second row* (Fig. 3, *C* and *D*) shows the data for the recovery from inactivation (traces from one representative cell are superimposed for the control (*line*), toxin (*line*), and the toxin-sensitive component (*open squares*). The *third row* (Fig. 3, *E* and *F*) shows the data for the voltage dependence of inactivation of the slow (○) and steady-state component (△) under control conditions (■) and at the highest concentration used. The *insets* show the superimposed recordings from a representative cell of the complete inactivation protocol under control conditions and at the highest concentration.

These data suggest that the action of AFT-II is similar to that of ATX-II and that Bc-III has a lower affinity for this type of channel. Interestingly, the results obtained with these two new toxins differ from those obtained with ATX-II, insofar, as there was a small supplementary persistent component characterized by right-shifted inactivation curves.

Similar procedures were used to analyze the data obtained with the three toxins acting on the Na^+ currents in the different cell lines expressing the $Na_v1.1$, $Na_v1.2$, $Na_v1.3$, $Na_v1.4$, and $Na_v1.6$ sodium channel genes as described in the subsequent paragraphs.

The effects of ATX-II, AFT-II, and Bc-III on $Na_v1.1$—The results of experiments on cells expressing the $Na_v1.1$ channel are shown in Fig. 4. In the nine panels, the data are divided in three columns for ATX-II ($n = 3$), AFT-II ($n = 4$), and Bc-III ($n = 4$). The *first row* (Fig. 4, *A–C*) shows the effect of

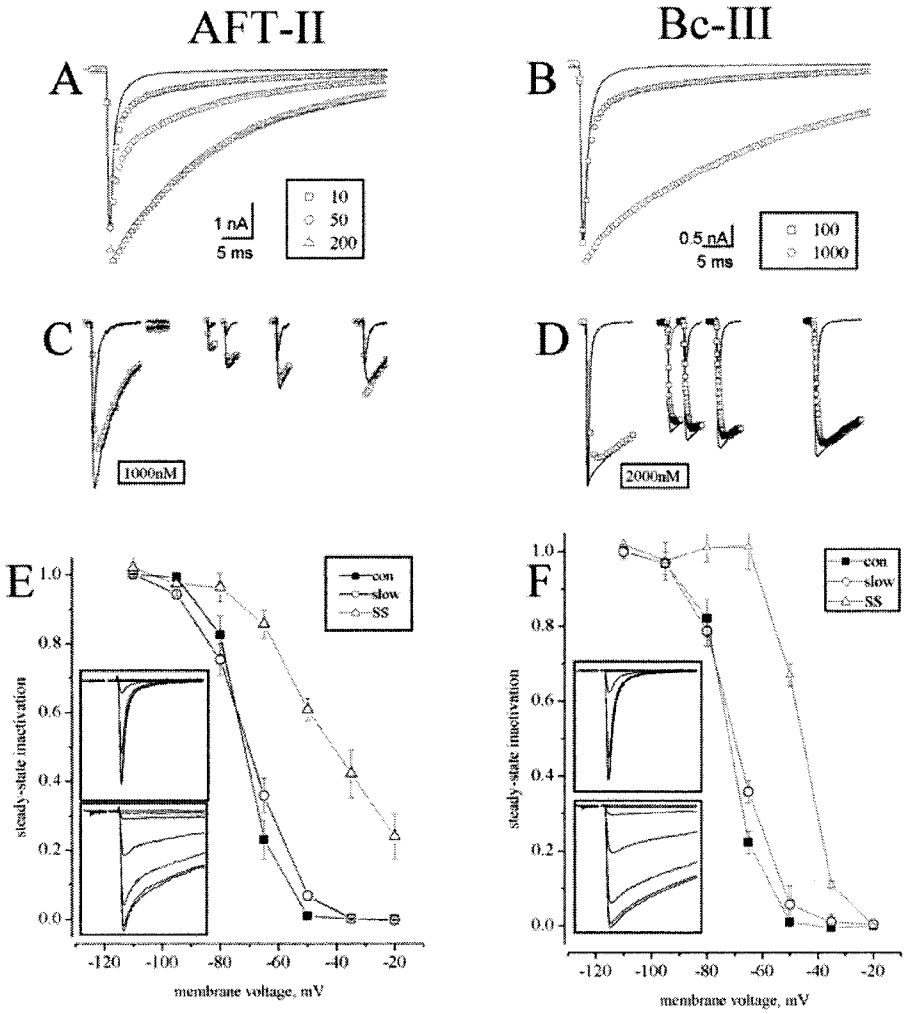

FIG. 3. **Effects of AFT-II and Bc-III on $Na_v1.5$ channels.** *A–B*, superimposed traces of the Na^+ currents elicited from −110 to −20 mV under control conditions and at the indicated concentrations (a single cell for each toxin). *C–D*, superimposed recordings of the Na^+ currents obtained during recovery from inactivation (see protocol in Fig. 2*F*) under control conditions and at the indicated toxin concentrations studied at −80 mV for 10, 20, 50, and 100 ms (*C*) and 5, 10, 20, and 50 ms (*D*). There is an axis break during the test pulse (duration 90 ms). The toxin and control traces are shown as *continuous lines*. The *line of circles* shows the difference between the two traces. *E–F*, steady-state inactivation in control (■) and the voltage dependence of the slow (○) and persistent component (△) during the application of 400 nM (*AFT-II*) and 2000 nM (*Bc-III*). Mean values ± S.E. (n = 5). The *insets* to these panels show the superimposed traces in the control (*top*) and toxin experiments (*bottom*). There is a time break in the first part of the trace showing the preconditioning levels. The *inward current traces* last for 15 ms.

different toxin concentrations (superimposed traces from a representative cell). The *second row* (Fig. 4, *D–F*) shows the data for the recovery from inactivation (superimposed traces from one representative cell in control, toxin, and the toxin-sensitive component). The *third row* (Fig. 4, *G–I*) shows the data for the voltage dependence of inactivation in the control (■) and slow (○) and steady-state components (△). The *insets* show the superimposed recordings from a representative cell for the complete inactivation protocol under control conditions and at the highest concentration used (note the break in the time axis).

The average time constant of the slow component (shown in Table II) did not depend on the toxin concentration or the preconditioning voltage (in the range −110/−50 mV). During preconditioning at −35 and −20 mV, AFT-II and Bc-III induced currents that were almost persistent but not present in the control and that did not inactivate when tested at −20 mV. These persistent components had a right-shifted voltage-dependent curve in comparison with the control and slow component behavior.

The Effects of ATX-II, AFT-II, and Bc-III on $Na_v1.2$—The results of experiments similar to those reported for $Na_v1.1$ are shown in Fig. 5 for $Na_v1.2$ channels. Once again, the action of ATX-II (n = 3) was seen at much lower concentrations than that of AFT-II and Bc-III (n = 4). Although at high concentrations ATX-II and Bc-III often led to a slight increase in peak currents with respect to control, the effect of AFT-II on peak currents was more marked (increase of the order of 60 ± 5.4% (n = 3)) and, in addition, a large persistent component was induced that was not inactivated at −20 mV (Fig. 5*H*, *insets*).

The Effects of ATX-II, AFT-II, and Bc-III on $Na_v1.3$—Similar experiments were also performed for the $Na_v1.3$ channel (see Fig. 6). The three toxins were effective only at relatively higher concentrations. As noted for $Na_v1.2$, only AFT-II induced a large increase in peak current (see Fig. 6*H*, *insets*). Persistent currents are typical of this channel. Only ATX-II led to a negatively shifted inactivation curve of the slow component.

The Effects of ATX-II, AFT-II, and Bc-III on $Na_v1.4$—The effect of the three toxins on the $Na_v1.4$ channel are shown in Fig. 7. The inactivation time constant under control conditions was 0.5 ± 0.15 ms (n = 7), but this increased ~10-fold following the application of the toxins. Nevertheless, the slow component time constants for $Na_v1.4$ are the lowest among the subtypes tested (see Table II). It is worth noting that both ATX-II and AFT-II induced a non-parallel leftward shift of the inactivation curve that was more pronounced toward the most negative region and that the recordings were devoid of any persistent component. Only Bc-III generated a small steady-state component.

The Effects of ATX-II, AFT-II, and Bc-III on $Na_v1.6$—Unlike those observed for the $Na_v1.5$ channels, the results obtained for $Na_v1.6$ channels (see Fig. 8) are similar to those found for $Na_v1.3$ channels including the appearance of a persistent component during activation, a remarkable right shift of voltage-dependent inactivation and the leftward shift of the slow component. This finding suggests that these ef-

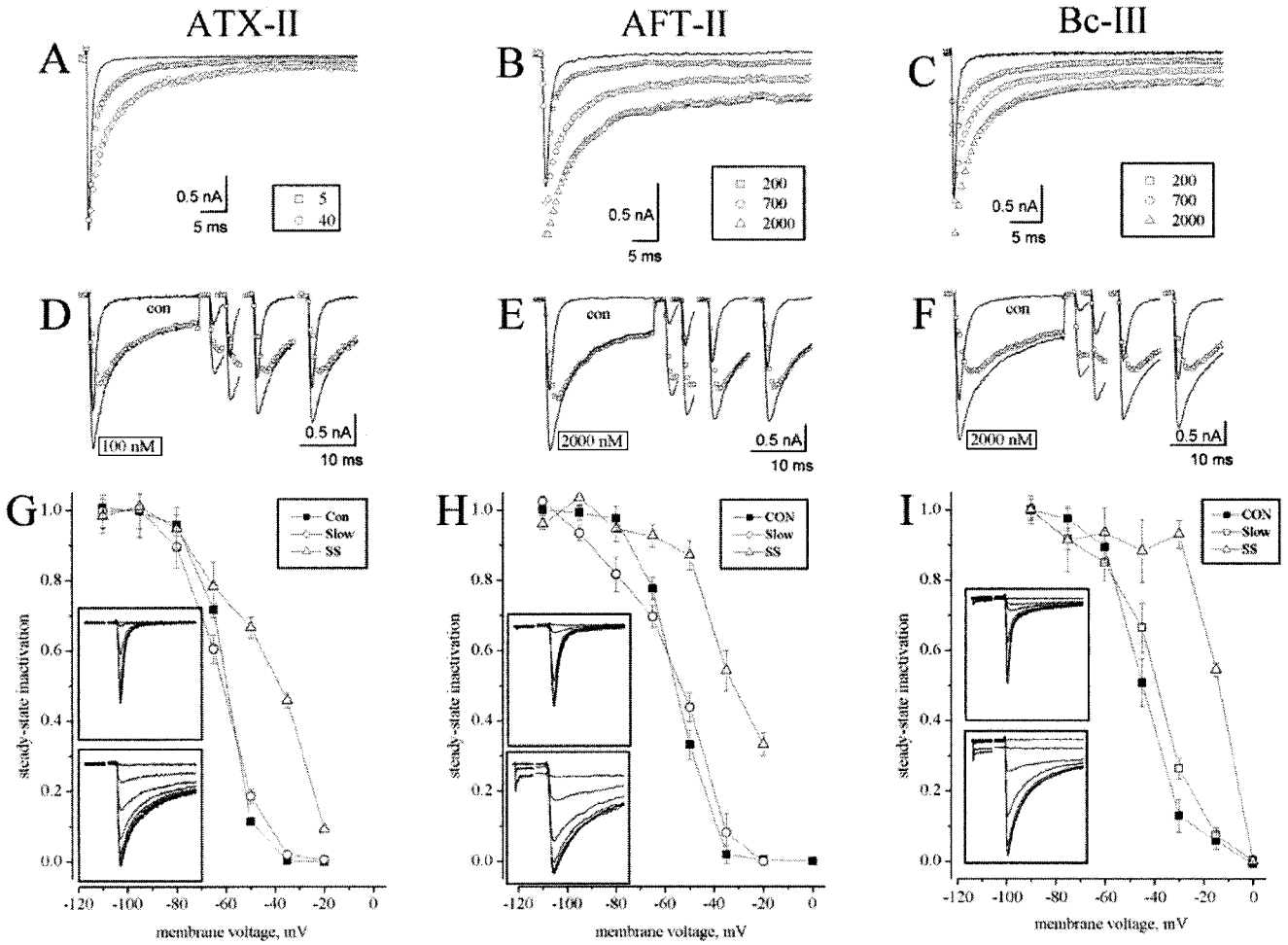

FIG. 4. **Effects of ATX-II, AFT-II, and Bc-III on Na$_v$1.1 channels.** *A–C*, superimposed traces of the Na^+ currents elicited from −110 to −20 mV under control conditions and at the indicated concentrations (a single cell for each toxin). *D–F*, superimposed recordings of the Na^+ currents obtained during recovery from inactivation studied at −80 mV for 2, 5, 10, and 20 ms (see protocol in Fig. 2*F*) under control and toxin conditions (*continuous line*, indicated concentration). The toxin and control traces are shown as *continuous lines*. The *line of squares* shows the difference between the two traces. *G–I*, steady-state inactivation in control (■) and the voltage dependence of the slow (○) and persistent component (△) during the application of 100 nM (*ATX-II*) and 2000 nM (*AFT-II* and *Bc-III*) (mean values ± S.E., n = 4). The *insets* to these panels show the superimposed control (*top*) and toxin traces (*bottom*). There is a time break in the first part of the trace showing the preconditioning levels. The *inward current traces* last for ~15 ms.

TABLE II
Inactivation and time constants

Time constants of the slow component, τ_{slow}, and voltage-shifts of the slow and steady-state components (SS) of voltage-dependent inactivation at maximal ATX-II, AFT-II, and Bc-III concentrations; n = 4–7; var = the concentration-dependent (ATX-II) time constants of the slow component (see inset to Fig. 2G); n.a. = not available.

	τ_{slow} (msec)			Voltage-dependent inactivation					
				Shift (Slow) (mV)			Shift (SS) (mV)		
	ATX-II	AFT-II	Bc-III	ATX-II	AFT-II	Bc-III	ATX-II	AFT-II	Bc-III
Na$_v$1.1	7 ± 1.1	13 ± 1.3	16 ± 2.1	n.a.	n.a.	6 ± 0.4	9 ± 0.6	15 ± 1.5	30 ± 2.8
Na$_v$1.2	12 ± 0.9	12.7 ± 1.1	13 ± 1.5	n.a.	n.a.	n.a.	15.2 ± 2.2	30 ± 3	13.2 ± 1
Na$_v$1.3	7.8 ± 0.6	11 ± 1.2	17 ± 2.1	−7 ± 1	n.a.	n.a.	22 ± 3.5	34 ± 6.1	13 ± 2.6
Na$_v$1.4	6.3 ± 0.8	4.5 ± 0.6	8.5 ± 1.6	−6.1 ± 1	−6.4 ± 0.9	n.a.	n.a.	n.a.	15.2 ± 2.5
Na$_v$1.5	Var	18 ± 1	31 ± 1.8	−11 ± 1	n.a.	n.a.	n.a.	30 ± 2.3	25 ± 1.8
Na$_v$1.6	9.8 ± 0.6	16 ± 1.3	11 ± 0.9	−8 ± 0.4	−5 ± 0.5	n.a.	30 ± 2.9	40 ± 5.6	38 ± 7

fects are less characteristic of the toxins themselves but are probably more related to the structure of the specific channel subtype. The effects of ATX-II on peak currents were considerable, whereas AFT-II and Bc-III induced only minor increases.

Comparative Effects of the Inactivation Process on the Whole Na$_v$ Series—In general (with the exception of Na$_v$1.5), the time constants of the toxin-induced slow inactivation component did not vary as a function of toxin concentration (see first three columns of Table II). It can be seen that Bc-III produced the relatively highest time constant values, but Na$_v$1.4 is an exception and Na$_v$1.2 was affected to the same extent by all three toxins.

The same table also shows the shifts (on the voltage axis) of the voltage-dependent inactivation curves for both the slow and the steady-state components. The shift of the slow component was almost always negative (with the exception of Bc-III on Na$_v$1.1), whereas the shifts of steady-state components were

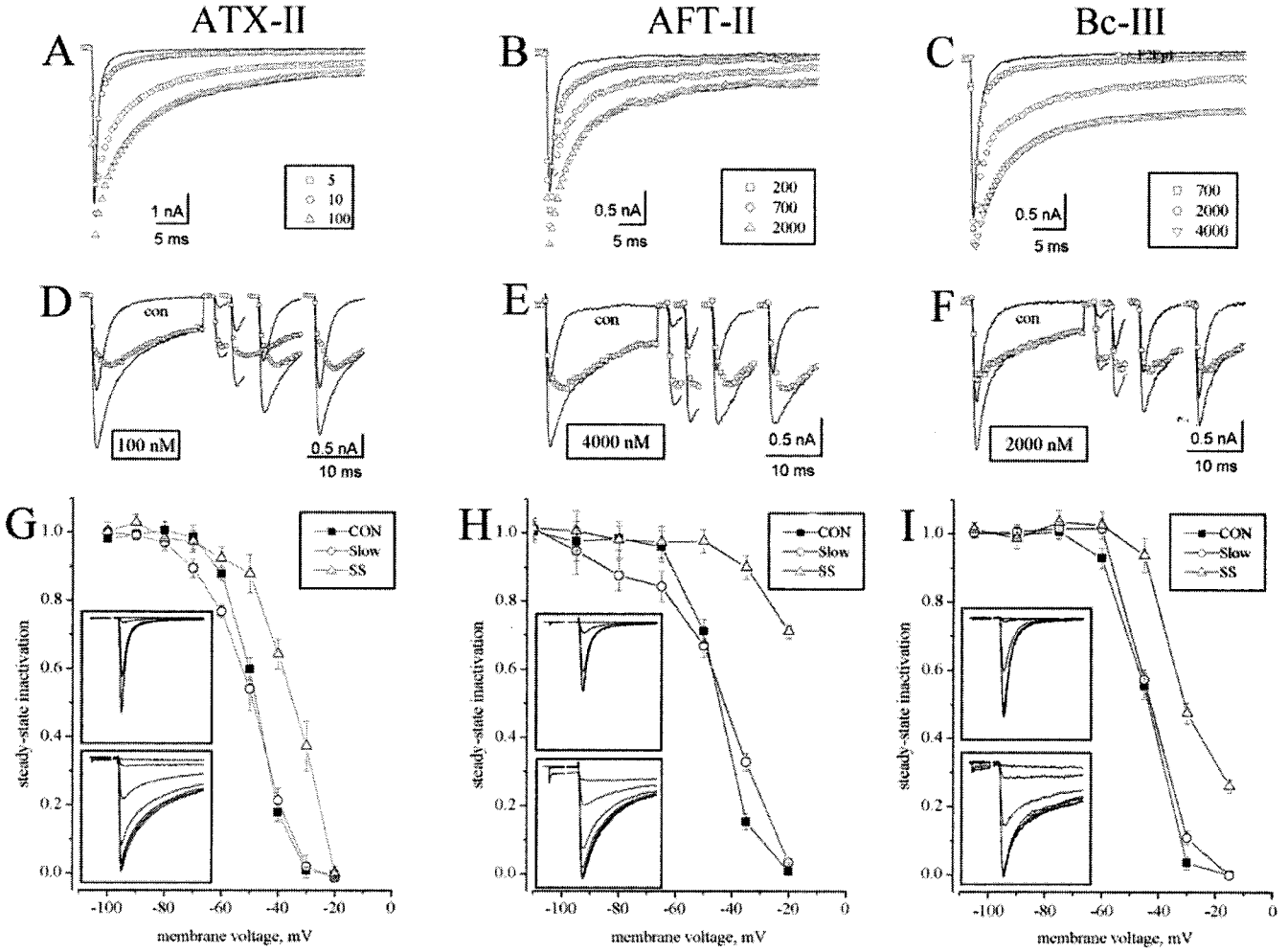

FIG. 5. **Effects of ATX-II, AFT-II, and Bc-III on $Na_v1.2$ channels.** *A–C*, superimposed traces of the Na^+ currents elicited from −110 to −20 mV under control conditions and at the indicated concentrations (a single cell for each toxin). *D–F*, superimposed recordings of the Na^+ currents obtained during recovery from inactivation (see protocol in Fig. 2*F*) under control conditions and at the indicated toxin concentrations studied at −80 mV for 2, 5, 10, and 20 ms. The toxin and control traces are shown as *continuous lines*. The *line of squares* shows the difference between the two traces. *G–I*, steady-state inactivation in control (■) and the voltage dependence of the slow (○) and persistent component (△) during the application of 100 nM (*ATX-II*), 4000 nM (*AFT-II*), and 2000 nM (*Bc-III*) (mean values ± S.E., $n = 4$). The *insets* to these panels show the superimposed control (*top*) and toxin traces (*bottom*). There is a time break in the first part of the trace showing the preconditioning levels. The *inward current traces* last for ~15 ms.

always positive (note that $Na_v1.6$ was greatly affected by the three toxins).

Dose-response Curves—To quantify and compare the effects of the three toxins on the various Na^+ channels, we evaluated the amplitude of the slow and steady-state toxin-induced components in relation to drug concentrations. All of the data were corrected for the amplitude of the slow component in the control recordings (normally <7–8%) and normalized to the control peak amplitude in each cell. The resulting dose-response curves (ATX-II (■), AFT-II (□), and Bc-III (○)) are shown in Fig. 9. We sometimes were unable to reach the maximal effect when the toxin potency was too low, because there was insufficient toxin material. Steady-state components were not observed with some subtypes, and the fact that this always led to a marked rightward shift of the inactivation curves suggests that this is probably due to changes in the biophysics of the channel as a result of binding to sites other than those responsible for slowing the inactivation. Simple visual inspection indicated that some dose-response curves were not sufficiently good to fit the classical logistic equation reasonably; thus only an approximate EC_{50} is given. For all of the other data, the results of the fitting procedure are shown in Table III for the slow component and Table IV for the steady-state component.

As shown in Table III, ATX-II is highly potent at $Na_v1.1$ and $Na_v1.2$ with an EC_{50} of ~7 nM ($n = 6$). In contrast AFT-II, which is only a single amino acid different, has only weak efficacy for these subtypes and has greatest efficacy for $Na_v1.4$ and $Na_v1.5$ (EC_{50} of ~30 and 62 nM, respectively). AFT-II and ATX-II had similar efficacies at both $Na_v1.5$ (~55 nM) and at $Na_v1.6$ (~240 nM). Bc-III has the lowest efficacy of all of the toxins with the greatest effects being on $Na_v1.1$ and $Na_v1.5$ (EC_{50} values of ~300 nM). In conclusion, the following EC_{50} rank order was found: ATX-II, $Na_v1.1$–$Na_v1.2 \ll Na_v1.5 < Na_v1.4 < Na_v1.6 < Na_v1.3$; AFT-II, $Na_v1.4 < Na_v1.5 < Na_v1.6 < Na_v1.3$–$Na_v1.1 < Na_v1.2$; and Bc-III, $Na_v1.5$–$Na_v1.1 < Na_v1.4$–$Na_v1.6 < Na_v1.2$–$Na_v1.3$.

The greatest efficacy (measured as the increase in the slow component) was obtained by AFT-II in the $Na_v1.3$ channel, 1.91 (as against 0.67 in $Na_v1.1$ and 1.42 in $Na_v1.2$) with 0.6 for the steady-state component. The toxins also induced large increases in this component in $Na_v1.6$.

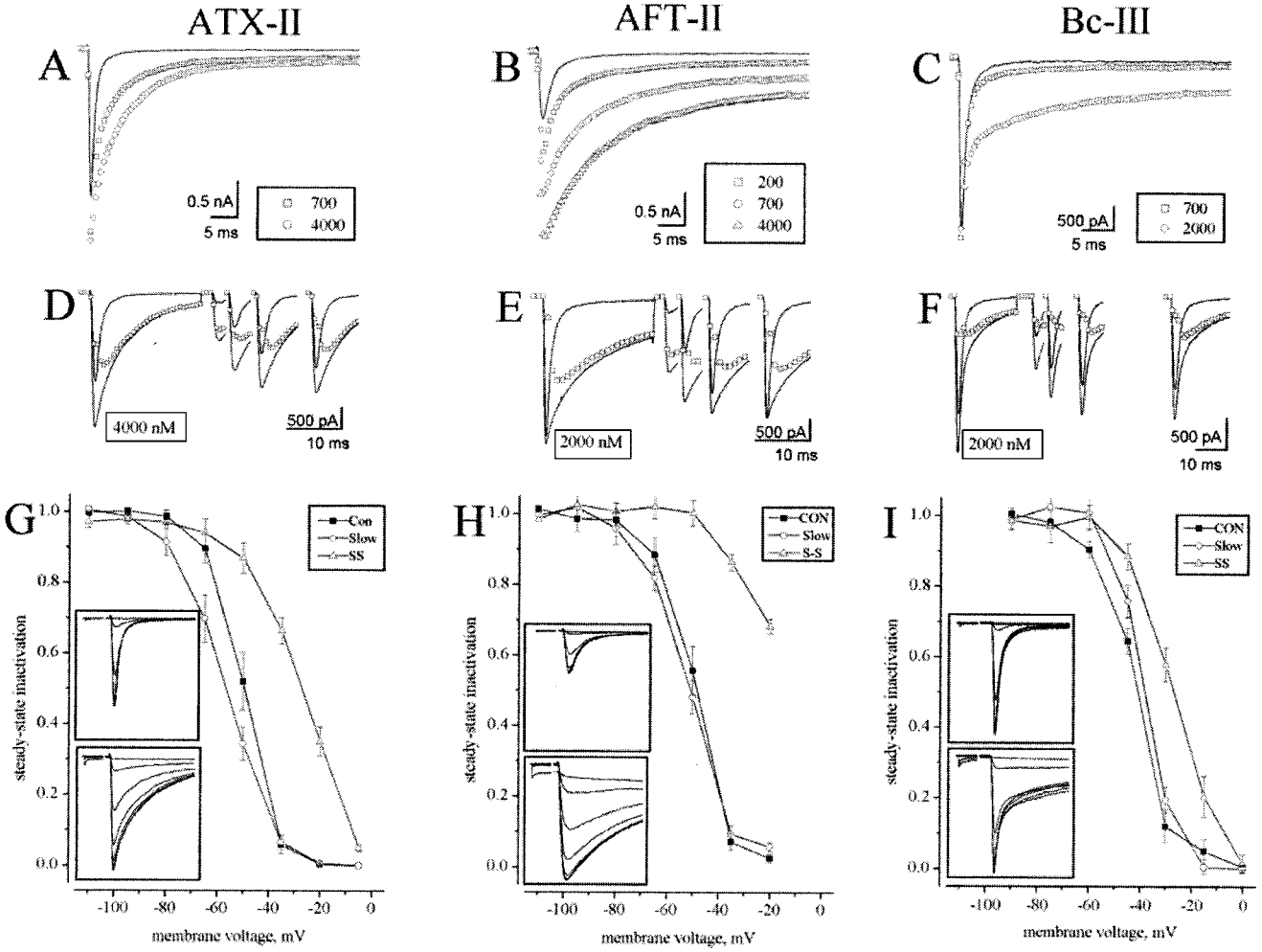

FIG. 6. **Effects of ATX-II, AFT-II, and Bc-III on $Na_v1.3$ channels.** *A–C*, superimposed traces of the Na^+ currents elicited from −110 to −20 mV under control conditions and at the indicated concentrations (a single cell for each toxin). *D–F*, superimposed recordings of the Na^+ currents obtained during recovery from inactivation (see Fig. 2*F*) under control conditions and at the indicated toxin concentrations studied at −80 mV for 2, 5, 10, and 20 ms. The toxin and control traces are shown as *continuous lines*. The *line of squares* shows the difference between the two traces. *G–I*, steady-state inactivation in control (■) and the voltage dependence of the slow (○) and persistent component (△) during the application of 4000 nM (*ATX-II*), 2000 nM (*AFT-II*), and 2000 nM (*Bc-III*) (mean values ± S.E., $n = 4$). The *insets* to these panels show the superimposed control (*top*) and toxin traces (*bottom*). There is a time break in the first part of the trace showing the preconditioning levels. The *inward current traces* last for ~15 ms.

DISCUSSION

Previous studies (3) of ATX-II have suggested that it is more specific for cardiac than skeletal muscle or brain voltage-gated Na^+ channels, but no specific gene was known at that time. ATX-II prolongs the duration of the cardiac action potential by increasing the functional contribution of the Na^+ current to the plateau (14) and has been used by a number of authors to investigate its ability to enhance persistent sodium currents (15, 16).

Detailed electrophysiological analyses of the different effects of sea anemone peptides on sodium channels have been reported (17–19), and various criteria have been used to produce comparative dose-response curves. Some authors have evaluated the increase in the amplitude of the toxin-induced slow component, and others have evaluated the value of the current after the completion of fast inactivation or the increase in the inactivation time constant 17–20. Because there is evidence indicating the co-existence of toxin-bound and toxin-free channels, we used the first criterion for both the toxin-induced slow and persistent components (see "Results") (20).

The changes in Na^+ channel kinetics induced by Bc-III and AFT-II have never been analyzed before, and we compared their effects on six Na^+ channel subtypes. These have highly related but differing amino acid sequences, such that differences in the effects of any given toxin should be directly attributed to these sequence variations. In considering this sequence variation, it should also be remembered that the α-subunit of Na^+ channels is normally complexed with the β-subunits, although it has been shown that the overexpression of the β_1-subunit in Chinese hamster ovary-expressing α-subunits does not alter the inactivation time constant (21). Moreover, it is known that β_{1A}-subunit mRNA is endogenously expressed in human embryonic kidney 293 cells (used in this study) (22). However, in our experiments, we did not investigate the effect of the β-subunits.

Different Potencies of the Same Toxin Caused by the Amino Acid Diversity of Na^+ Channels at the IV/S3-S4 Loop Domain—The results of site-directed mutagenesis studies have suggested that sea anemone toxins (and the α-toxins purified from scorpions that induce similar actions) interact with a glutamic acid residue (Glu-1613 in $Na_v1.2$) on the extracellular S3-S4 loop of the fourth domain of the rat neuronal channel $Na_v1.2$ (see Table V) (23). Table V shows that this amino acid has an aspartic change in cardiac, muscle, and other channels ($Na_v1.5$, $Na_v1.4$, $Na_v1.6$, and $Na_v1.7$). Furthermore, Glu-1616 also has a change in glutamine in $Na_v1.4$ and $Na_v1.5$. The authors found

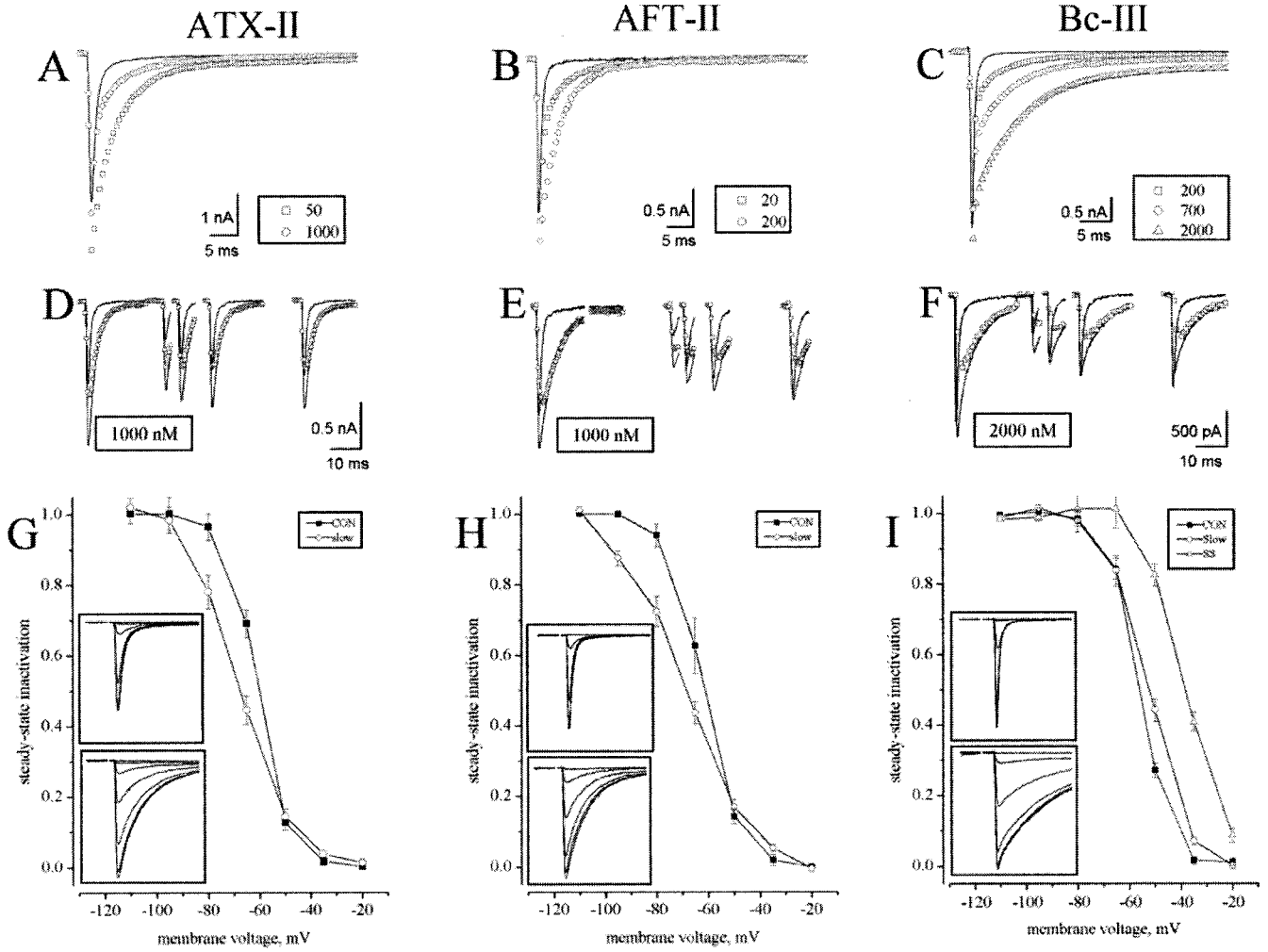

FIG. 7. **Effects of ATX-II, AFT-II, and Bc-III on $Na_v1.4$ channels.** *A–C*, superimposed traces of the Na^+ currents elicited from −110 to −20 mV under control conditions and at the indicated concentrations (a single cell for each toxin). *D–F*, superimposed recordings of the Na^+ currents obtained during recovery from inactivation (see protocol in Fig. 2*F*) under control conditions and at the indicated toxin concentrations studied at −80 mV for 2, 5, 10, and 20 ms (5, 10, 20, and 50 ms for *AFT-II* in *panel E*). The toxin and control traces are shown as *continuous lines*. The *line of squares* shows the difference between the two traces. *G–I*, steady-state inactivation in control (■) and the voltage dependence of the slow (○) and persistent component (△) during the application of 1000 nM (*ATX-II*), 1000 nM (*AFT-II*), and 2000 nM (*Bc-III*) (mean values ± S.E., $n = 5$). The *insets* to these panels show the superimposed control (*top*) and toxin traces (*bottom*). There is a time break in the first part of the trace showing the preconditioning levels. The *inward current traces* last for ~15 ms.

that the E1613D mutation significantly increased the affinity of ATX-II from 76 to 13 nM and that the E1616Q mutation had the opposite effect (from 76 to 163 nM). Unfortunately, they did not show the results of both mutations but suggest that the conversion of Glu-1613 or Glu-1616 to more negative/positive side chains increased/decreased ATX-II affinity, respectively, and thus proposed a model for electrostatic interaction between the acidic residues of the channel and the basic residues of the toxin.

As these changes occur simultaneously in $Na_v1.4$ and $Na_v1.5$, our EC_{50} data of 109 and 49 nM in $Na_v1.4$ and $Na_v1.5$ in comparison with ~7 nM in $Na_v1.2$ suggest that decreasing affinity is the prevalent effect.

Unexpectedly, $Na_v1.6$, which has only the first glutamate changed in aspartate in position 1604, also had no higher affinity for ATX-II. This channel is significantly more similar to $Na_v1.1/2$, because it has the single Asp-Ile motif (also in $Na_v1.5$) instead of the Glu-Leu motif present in $Na_v1.1/2$, thus suggesting a further determinant of toxin binding. Interestingly, $Na_v1.4$, which is less affected by ATX-II than $Na_v1.5$, has the Asp-Ile instead of the Asp-Ile motif, but the leucine is exactly the same amino acid as it is in $Na_v1.1/2$.

In comparison with $Na_v1.1/2$, the much lower potency of ATX-II in $Na_v1.3$ may be explained by the fact that neighboring amino acids can negatively manipulate the binding. The single change of a leucine to a methionine residue is precisely near Glu-1608 (in $Na_v1.3$), which is consistent with the idea that a longer side chain (Met instead of Leu) should induce a lower affinity for ATX-II (23).

AFT-II mainly affects the $Na_v1.4$ and $Na_v1.5$ channels and has much less potent effects on the other channels. Given the single amino acid difference (K36A) between ATX-II and AFT-II, these findings strongly support the idea that the lysine in position 36 is crucial for the very strong effects of ATX-II on $Na_v1.1/2$ channels.

Bc-III has a different amino acid sequence from that of ATX-II and AFT-II (see Table I) in both the critical positions of 12–14 and 35–37, which probably explains why it is less effective than ATX-II.

It is very interesting that a previous report (24) has shown that sea anemone BgII (from *Bunodosoma granulifera*) and α-scorpion toxins have a common distribution of positively charged patches in their three-dimensional structures. If we analyze the recent review by Mouhat *et al.* (29), the fundamen-

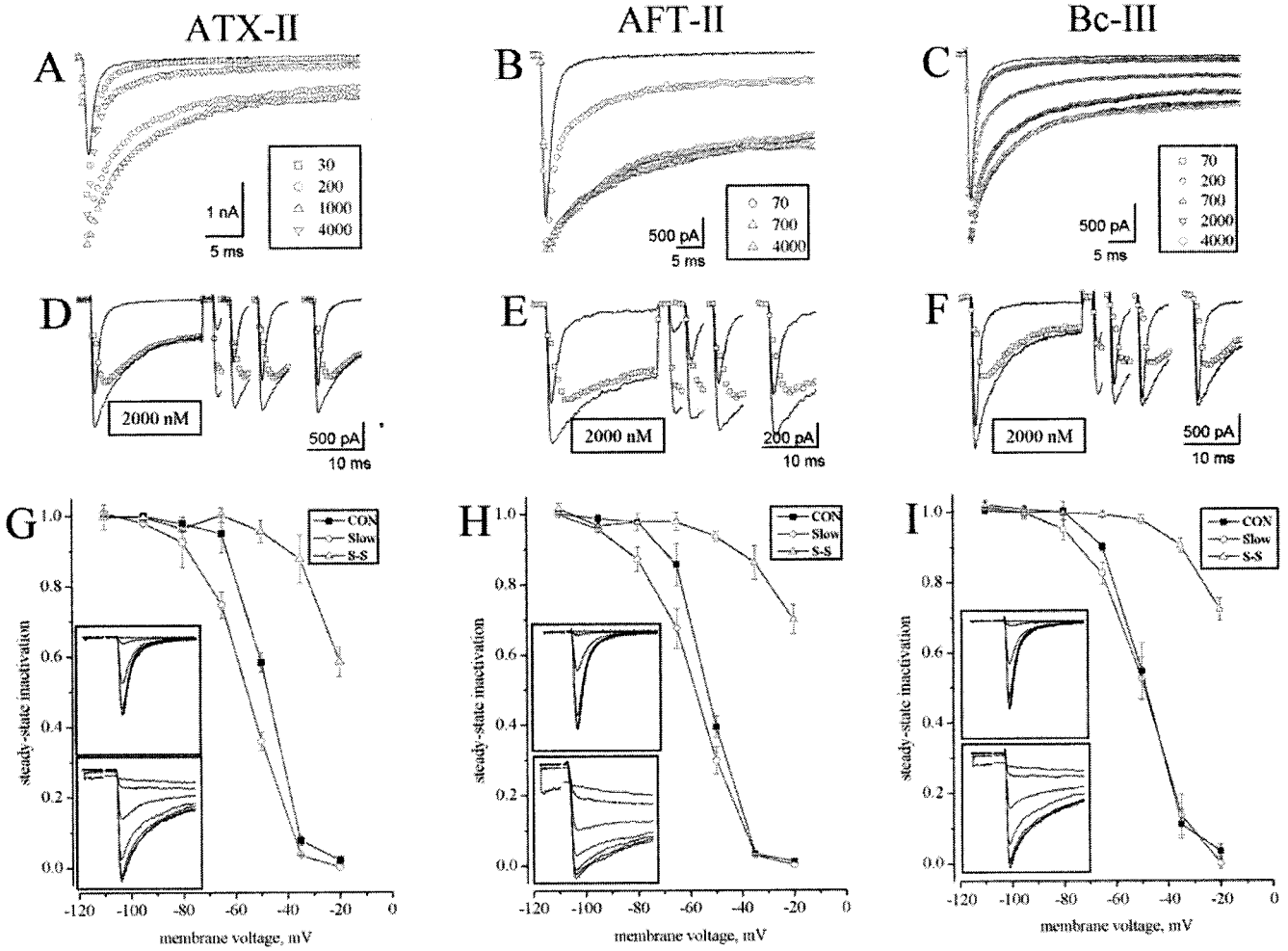

FIG. 8. **Effects of ATX-II, AFT-II, and Bc-III on $Na_v1.6$ channels.** *A–C*, superimposed traces of the Na^+ currents elicited from −110 to −20 mV under control conditions and at the indicated concentrations (a single cell for each toxin). *D–F*, superimposed recordings of the Na^+ currents obtained during recovery from inactivation (see protocol in Fig. 2*F*) under control conditions and at the indicated toxin concentrations studied at −80 mV for 2, 5, 10, and 20 ms. The toxin and control traces are shown as *continuous lines*. The *line of squares* shows the difference between the two traces. *G–I*, steady-state inactivation in control (■) and the voltage dependence of the slow (○) and persistent component (△) during the application of a toxin concentration of 2000 nM (mean values ± S.E., $n = 4$). The *insets* to these panels show the superimposed control (*top*) and toxin traces (*bottom*). There is a time break in the first part of the trace showing the preconditioning levels. The *inward current traces* last for ~15 ms.

tal Arg-14 and the patch of Glu-35, Glu-36, and Arg-37 of ATX-I (*A. sulcata*) (corresponding to the positive patch of Lys-35, Lys-36, and His-37 of ATX-II) should be localized in the loop between the first and the second β-sheets and between the third and the fourth β-sheets of the structure determined by NMR (25). This peculiar structural arrangement is located near the amino acids Arg-14, Lys-35, Lys-36, and His-37 of ATX-II, and it might be inferred that this strong positive patch plays a crucial role in binding the toxin to the negative residues of the IV/S3-S4 loop. Losses in the positive charges in this region strongly suggest losses in affinity.

Accordingly, Bc-III (the other new toxin tested) has much less potent effects on all of the investigated channels. On the other hand, BgII and BgIII, which are toxins similar to Bc-III, have been shown to affect the duration of the cardiac action potentials with the EC_{50} of 60 and 660 nM, respectively (18). However, in transfected *Xenopus laevis* oocytes expressing the $Na_v1.5$ channel, these EC_{50} become 380 and 7800 nM, respectively. BgII and BgIII have only one difference (N16D) thought to be important for toxicity, and Bc-III has the same asparagine in position 16 and therefore can be considered much more similar to BgII than BgIII. In transfected *X. laevis* oocytes expressing both $Na_v1.5/\beta_1$ and $Na_v1.2/\beta_1$, Bosmans *et al.* (26) demonstrate a potency ranking of $Na_v1.2/\beta_1 > Na_v1.5/\beta_1 > Na_v1.4/\beta_1$, which is different from that reported here probably because of the presence of the β-subunit or the different cell type.

On the whole, it is our opinion that, as the majority of the results qualitatively reinforce the important role of the S3-S4 loop of domain IV, other regions are probably also important. This is substantiated by the fact that $Na_v1.6$ has conserved acidic residues in both positions 1605 and 1608 ($Na_v1.6$ numbering) and long side chain amino acids in between. But ATX-II and AFT-II have only moderate efficacy, thus suggesting that interactions with other regions of the channel are different with respect to $Na_v1.1/2$.

Different Potency on the Same Na^+ Channel Caused by the Amino Acid Diversity of the Toxins—The suggestion that either Glu or Asp at the beginning of the IV/S3-S4 loop is important for sea anemone toxin binding has been further investigated by other authors (27–29) who modified the toxin peptide. The results of extensive site-directed mutagenesis studies of ApB purified from *Anthopleura xanthogrammica* sea anemone indicate that Arg-12 and Arg-14 are critical for affinity (27, 28), but it has more recently been shown by Benzinger *et al.* (13) that the Lys-37 position of ApB interacts with the Asp-1610 of

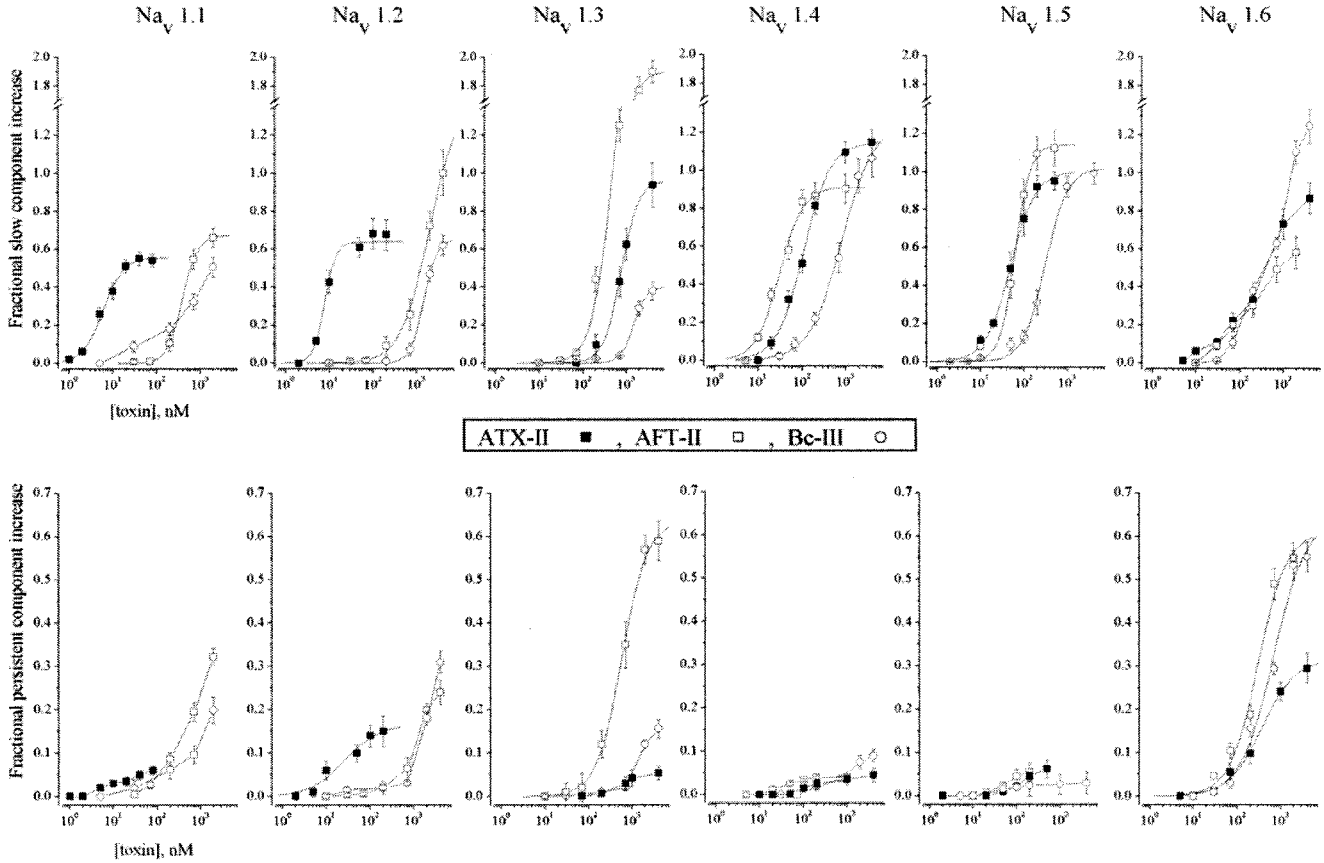

FIG. 9. **Dose-response relationships of the increase in the slow and persistent components of the different channel types.** *Upper* and *lower graphs*, respectively, show the plots of the fractional increases in the slow and persistent components (note the different *y* scale). The different toxins are shown with the indicated symbols.

TABLE III

Dose-response curve data for the fractional increase in the slow component

When possible and reasonable, the data were analyzed on the basis of the logistic function $A/(1 + (EC_{50}/[toxin])^p$. Otherwise, only a rough estimate of the EC_{50} is given. The fitting parameters were A (maximal effect), EC_{50} (nM), and p (power) (n = 4–6 cells for each toxin and each channel type). n.a. = not applicable.

		ATX-II	AFT-II	Bc-III
$Na_v1.1$	A	0.56 ± 0.02	0.67 ± 0.02	Estimated ~ 0.6
	EC_{50}	6.01 ± 0.46	390.55 ± 30.75	Estimated ~ 300
	p	1.86 ± 0.09	2.46 ± 0.24	n.a.
$Na_v1.2$	A	0.64 ± 0.02	1.42 ± 0.22	0.65 ± 0.08
	EC_{50}	7.88 ± 0.48	1998 ± 519.3	1449.17 ± 216.47
	p	3.33 ± 0.41	1.31 ± 0.11	2.86 ± 0.64
$Na_v1.3$	A	0.96 ± 0.09	1.91 ± 0.07	0.4 ± 0.02
	EC_{50}	759.22 ± 99.9	459.36 ± 48.13	1458.42 ± 128.52
	p	2.13 ± 0.37	1.85 ± 0.12	2.93 ± 0.51
$Na_v1.4$	A	1.15 ± 0.03	0.91 ± 0.04	1.26 ± 0.09
	EC_{50}	109.49 ± 7.01	30.62 ± 3.46	820.84 ± 144.31
	p	1.41 ± 0.12	1.64 ± 0.23	1.16 ± 0.13
$Na_v1.5$	A	1 ± 0.03	1.14 ± 0.04	1.02 ± 0.04
	EC_{50}	49.05 ± 3.31	62.5 ± 4.05	307 ± 32.5
	p	1.52 ± 0.12	2.5 ± 0.42	1.72 ± 0.21
$Na_v1.6$	A	Estimated ~ 0.9	Estimated ~ 0.65	Estimated ~ 1.4
	EC_{50}	Estimated ~ 180	Estimated ~ 300	Estimated ~ 900
	p	n.a.	n.a.	n.a.

$Na_v1.5$ (corresponding to the Glu-1613 of $Na_v1.2$). They specifically found that the change, D1610R, causes a 100-fold increase in toxin K_D. Moreover, a toxin mutation (K37A) caused a 10-fold K_D increase in the wild type channel and a much smaller increase in the D1610R channel mutant.

In ATX-II and AFT-II, the corresponding Lys is in position 35 and preceded by a well preserved structure that is common to all of the toxins. The following amino acids (position 36) is also a Lys in ATX-II but is changed to an Ala in AFT-II (the only difference between the two toxins). AFT-II and ApB are equal in this region, and therefore, our studies may elucidate the importance of this hypothesized toxin-channel interaction.

We found that AFT-II and ATX-II are equally potent on $Na_v1.5$ (EC_{50} of ~55 nM), in reasonable agreement with Benzinger ApB affinity data and the hypothesis of the crucial role of Lys-37. On the contrary, it is not at all confirmed in $Na_v1.1/2/3$ because ATX-II is significantly more potent than AFT-II on the first two channels but less potent than AFT-II on $Na_v1.3$.

TABLE IV
Dose-response curve data for the fractional increase in the steady-state component

The same parameters as in Table 3.

		ATX-II	AFT-II	Bc-III
$Na_v1.2$	A	0.17 ± 0.03	n.a.	n.a.
	EC_{50}	26.9 ± 16.47		
	p	1.1 ± 0.4		
$Na_v1.3$	A	n.a.	0.64 ± 0.02	n.a.
	EC_{50}		580.32 ± 51.7	
	p		1.48 ± 0.14	
$Na_v1.6$	A	0.32 ± 0.02	0.61 ± 0.07	0.64 ± 0.08
	EC_{50}	368.72 ± 56.71	301.9 ± 85.5	683.3 ± 210.6
	p	1.13 ± 0.12	1.33 ± 0.32	1.15 ± 0.24

TABLE V
Position and aminoacid sequences of $Na_v1.1$–7 channels in the segment 3 and 4 extracellular loop of the IV domain

Identical amino acids have a white background; homologous amino acids have a gray background; and different amino acids have a black background.

		IVS3									Loop									IVS4		
Position																						
Nav1.1	(1616)	I	V	G	M	F	L	A	E	L	I	E	K	Y	F	V	S	P	T	L	F	R	V	I
Nav1.2	(1606)	I	V	G	M	F	L	A	E	L	I	E	K	Y	F	V	S	P	T	L	F	R	V	I
Nav1.3	(1601)	I	V	G	M	F	L	A	E	M	I	E	K	Y	F	V	S	P	T	L	F	R	V	I
Nav1.4	(1628)	I	V	G	L	A	L	S	D	L	I	Q	K	Y	F	V	S	P	T	L	F	R	V	I
Nav1.5	(1603)	I	V	G	T	V	L	S	D	I	I	Q	K	Y	F	F	S	P	T	L	F	R	V	I
Nav1.6	(1597)	I	V	G	M	F	L	A	D	I	I	E	K	Y	F	V	S	P	T	L	F	R	V	I
Nav1.7	(1579)	I	V	G	M	F	L	A	D	L	I	E	T	Y	F	V	S	P	T	L	F	R	V	I

Because the only difference between the two toxins is the K36A mutation and $Na_v1.1$ and $Na_v1.2$ are also identical in that region, it is necessary to attribute a crucial function to Lys-36, at least in $Na_v1.1/2$, and not to Lys-35. This finding suggests that the neighboring amino acids of the toxin may be critical for the binding.

Furthermore, because $Na_v1.4$ is only marginally different from $Na_v1.5$ in this region, although $Na_v1.5$ has a Phe residue in position 1617 instead of the Val in all of the other channels, we expected to find that the action of ATX-II and AFT-II would be similar. However, we found that AFT-II is more potent than ATX-II (EC_{50} of 30.62 ± 3.46 *versus* 109.49 ± 7 nM), which may indicate that the amino acid 1611 after Asp-1610, which is Leu in $Na_v1.4$ instead of Ile, is important for binding or that other residues are crucial in other regions.

Although previous observations and Benzinger data seem to confirm the importance of Asp-1610 in $Na_v1.5$, the same amino acid is also present in $Na_v1.6$ (followed by an Ile as in $Na_v1.5$) but AFT-II and ATX-II are approximately five times less potent in this channel type. On the other hand, the previous amino acid in $Na_v1.5$ is a polar Ser instead of the aliphatic Ala present in all of the other channels. Therefore, we are again forced to conclude that the adjacent amino acids should be crucial because it is confirmed by the dose-response data in $Na_v1.4$, which is much more similar to $Na_v1.5$ than to $Na_v1.6$.

During our experiments, we found that the toxins only sometimes induce a prominent steady-state component, which has a pronounced right-shifted inactivation characterized by a persistent component at potentials of approximately −30/−20 mV. In relation to the steady-state component, two effects can be distinguished. Toxins are especially strong on this aspect, and channels are especially prone to be affected in this way. AFT-II was capable of causing this effect to a large extent, and $Na_v1.3$ and $Na_v1.6$ responded with a large steady-state component. This finding suggests that the amino acid pattern in region 35–36 of the toxin can cause a supplementary alteration that leads to the persistent component.

The fact that ATX-II is less potent in inducing slow inactivation in $Na_v1.3$ than AFT-II may be related to its ability to produce the persistent component in $Na_v1.3$. On the whole, both effects should suggest an alternative explanation, that the toxins do not bind the $Na_v1.3$ channel in the same position (Glu) as ATX-II does in $Na_v1.1$ and $Na_v1.2$.

Concluding Remarks—Billions of years of evolution have randomly led to the existence of a family of closely related mammalian sodium channel subtypes and to the selection of an array of peptide toxins produced by predatory animals that exert their effects upon these channels. The study of these natural variants is a complementary approach to site-directed mutagenesis that will help define their mutual interactions and should lead to an understanding of the structure, function, and mechanism of action of both the channels and the toxins themselves.

This study is restricted to the effects of the toxins on recombinant Na_V channel subtypes, *i.e.* a prolongation and increase of the currents were observed. The physiological consequences of this gain-of-function effect with respect to neuronal firing properties, propagation, and contraction of skeletal muscle cells and cardiac action potential duration remain to be determined if we are to fully understand the functional impact of these toxins.

Acknowledgments—We thank Dr. Izaura Yoshico Hirata of the Department of Biophysics (UNIFESP, São Paulo, Brazil) for confirming the amino acid sequences and Dr. Fernanda C. V. Portaro of the CAT/CEPID-FAPESP Butantan Institute (São Paulo, Brazil) for assistance with the purification procedures. We are profoundly indebted to Dr. M. Mantegazza of the C. Besta National Neurological Institute (Milan, Italy) for suggesting the use of clonal cell lines and Dr. Koji Muramoto of the Department of Biological Science at Tohoku University for providing us with AFT-II. We also thank Drs Emanuele Schiavon and Michela Chatel for the cell cultures and G. Mostacciuolo for technical improvements. J. S. O. amd A. J. Z. are Ph.D. students at the Physiology Department of the Biosciences Institute of the University of São Paulo. E. R. and R. R. C. are Ph.D. students of Physiology at the Department of Biotechnology and Biosciences of the University of Milan-Bicocca.

REFERENCES

1. Cestèle, S., and Catteral, W. A. (2000) *Biochimie* (*Paris*) **82,** 883–892
2. Catteral, W. A., Chandy, K. G., and Gutman, G. A. (2002) *The IUPHAR Compendium of Voltage-gated Ion Channels*, IUPHAR Media, Leeds, United Kingdom
3. Béress, L., Béress, R., and Wunderer, G. (1975) *FEBS Lett.* **50,** 311–314
4. Sunahar, S., Muramoto, K., Tenma, K., and Kamiya, H. (1987) *Toxicon* **25,** 211–219
5. Malpezzi, E. L. A., Freitas, J. C., Muramoto, K., and Kamiya, H. (1993) *Toxicon* **31,** 853–864
6. Lanio, M. E., Morera, V., Alvarez, C., Tejuca, M., Gómez, T., Pazos, F., Besada, V., Martínez, D., Huerta, V., Padrón, G., and Chávez, M. A. (2001) *Toxicon* **39,** 187–194
7. Meier, J., and Theakston, R. D. G. (1986) *Toxicon* **24,** 395–401
8. Rees, S., Coote, J., Stables, J., Goodson, S., Harris, S., and Lee, M. G. (1996) *BioTechniques* **20,** 102–110
9. Chen, Y. H., Dale, T. J., Romanos, M. A., Whitaker, W. R., Xie, X. M., and Clare, J. J. (2000) *Eur. J. Neurosci.* **12,** 4281–4289
10. Burbidge, S. A., Dale, T. J., Powell, A. J., Whitaker, W. R., Xie, X. M., Romanos, M. A., and Clare, J. J. (2002) *Mol. Brain Res.* **103,** 80–90
11. Xie, X. M., Dale, T. J., John, H. L., Cater, T. C., Peakman, T. C., and Clare, J. J. (2001) *Pfluegers Arch. Eur. J. Physiol.* **441,** 425–433
12. Faravelli, L., Arcangeli, A., Olivotto, M., and Wanke, E. (1996) *J. Physiol.* (*Lond.*) **496,** 13–23
13. Benzinger, G. R., Kyle, J. W., Blumenthal, K. M., and Hanck, D. A. (1998) *J. Biol. Chem.* **273,** 80–84
14. Romey, G., Renaud, J. F., Fosset, M., and Lazdunski, M. (1980) *J. Pharmcol. Exp. Ther.* **213,** 607–615
15. Brand, S., Seeger, T., and Alzheimer, C. (2000) *Eur. J. Neurosci.* **12,** 2387–2396
16. Mantegazza, M., Franceschetti, S., and Avanzini, G. (1998) *J. Physiol.* (*Lond.*) **507,** 105–116
17. Chahine, M., Plante, E., and Kallen, R. G. (1996) *J. Membr. Biol.* **152,** 39–48
18. Goudet, C., Ferrer, T., Galab, L., Artiles, A., Batista, C. F. V., Possani, L., Alvarez, J., Aneiros, A., and Tytgat, J. (2001) *Br. J. Pharmacol.* **134,** 1195–1206
19. Salceda, E., Garateix, A., and Soto, E. (2002) *J. Pharmacol. Exp. Ther.* **303,**

1067–1074
20. Chen, H. C., Lu, S. Q., Leipèold, E., Gordon, D., Hansel, A., and Heinemann, S. H. (2002) *Eur. J. Neurosci.* **16,** 767–770
21. Isom, L. I., Scheuer, T., Brownstein, A. B., Ragsdale, D. S., Murphy, B. J., and Catteral, W. A. (1995) *J. Biol. Chem.* **17,** 3306–3312
22. Moran, O., Nizzari, M., and Conti, F. (2000) *FEBS Lett.* **473,** 132–134
23. Rogers, J. C., Qu, Y. S., Tanada, T. N., Scheuer, T., and Catteral, W. A. (1996) *J. Biol. Chem.* **271,** 15950–15962
24. Loret, E. P., del Valle, R. M., Mansuelle, P., Sampieri, F., and Rochat, H. (1994) *J. Biol. Chem.* **269,** 16785–16788
25. Widmer, H., Billeter, M., and Wuthrich, K. (1989) *Proteins* **6,** 357–371
26. Bosmans, F., Aneiros, A., and Tytgat, J. (2002) *FEBS Lett.* **532,** 131–134
27. Gallagher, M. J., and Blumenthal, K. M. (1994) *J. Biol. Chem.* **269,** 254–259
28. Khera, P. K., and Blumenthal, K. M. (1996) *Biochemistry* **35,** 3503–3507
29. Mouhat, S., Jouirou, B., Mosbah, A., De Waard, M., and Sabatier, J. (2004) *Biochem. J.* **378,** 717–726

Binding Specificity of Sea Anemone Toxins to Na_V 1.1-1.6 Sodium Channels: UNEXPECTED CONTRIBUTIONS FROM DIFFERENCES IN THE IV/S3-S4 OUTER LOOP

Joacir Stolarz Oliveira, Elisa Redaelli, André J. Zaharenko, Rita Restano Cassulini, Katsuhiro Konno, Daniel C. Pimenta, José C. Freitas, Jeffrey J. Clare and Enzo Wanke

J. Biol. Chem. 2004, 279:33323-33335.
doi: 10.1074/jbc.M404344200 originally published online May 28, 2004

THE JOURNAL OF BIOLOGICAL CHEMISTRY
Vol. 279, No. 42, Issue of October 15, pp. 44229–44230, 2004

Printed in U.S.A.

Additions and Corrections

Vol. 279 (2004) 33123–33130

MalK, the ATP-binding cassette component of the *Escherichia coli* maltodextrin transporter, inhibits the transcriptional activator MalT by antagonizing inducer binding.

Nicolas Joly, Alex Böhm, Winfried Boos, and Evelyne Richet

Page 33124, lines 7 and 8 under "Experimental Procedures": The name and sequence of the upstream primer used to amplify the *malK* gene, rather than KU001 (5′-GCGGCGCCATGGGGACCCACGATCAGGTCGA-3′, should be: KU006 (5′-CGCCGCGCCATGGGGATGGCGAGCGTACAGCTGC-3′).

Vol. 279 (2004) 33323–33335

Binding specificity of sea anemone toxins to Na_v 1.1–1.6 sodium channels. Unexpected contributions from differences in the IV/S3-S4 outer loop.

Joacir Stolarz Oliveira, Elisa Redaelli, André J. Zaharenko, Rita Restano Cassulini, Katsuhiro Konno, Daniel C. Pimenta, José C. Freitas, Jeffrey J. Clare, and Enzo Wanke

Page 33323, line 10 of the summary: L36A should be changed to K36A.

Page 33331, next to the last line in the left-hand column: The first Asp-Ile should be changed to Asp-Leu, to read "The Asp-Leu instead of the Asp-Ile motif . . ."

We suggest that subscribers photocopy these corrections and insert the photocopies at the appropriate places where the article to be corrected originally appeared. Authors are urged to introduce these corrections into any reprints they distribute. Secondary (abstract) services are urged to carry notice of these corrections as prominently as they carried the original abstracts.

Vol. 279 (2004) 31041–31049

R-cadherin influences cell motility via Rho family GTPases.

Emhonta Johnson, Christopher S. Theisen, Keith R. Johnson, and Margaret J. Wheelock

Page 31046: The wrong Fig. 5 was printed. The correct figure is shown below:

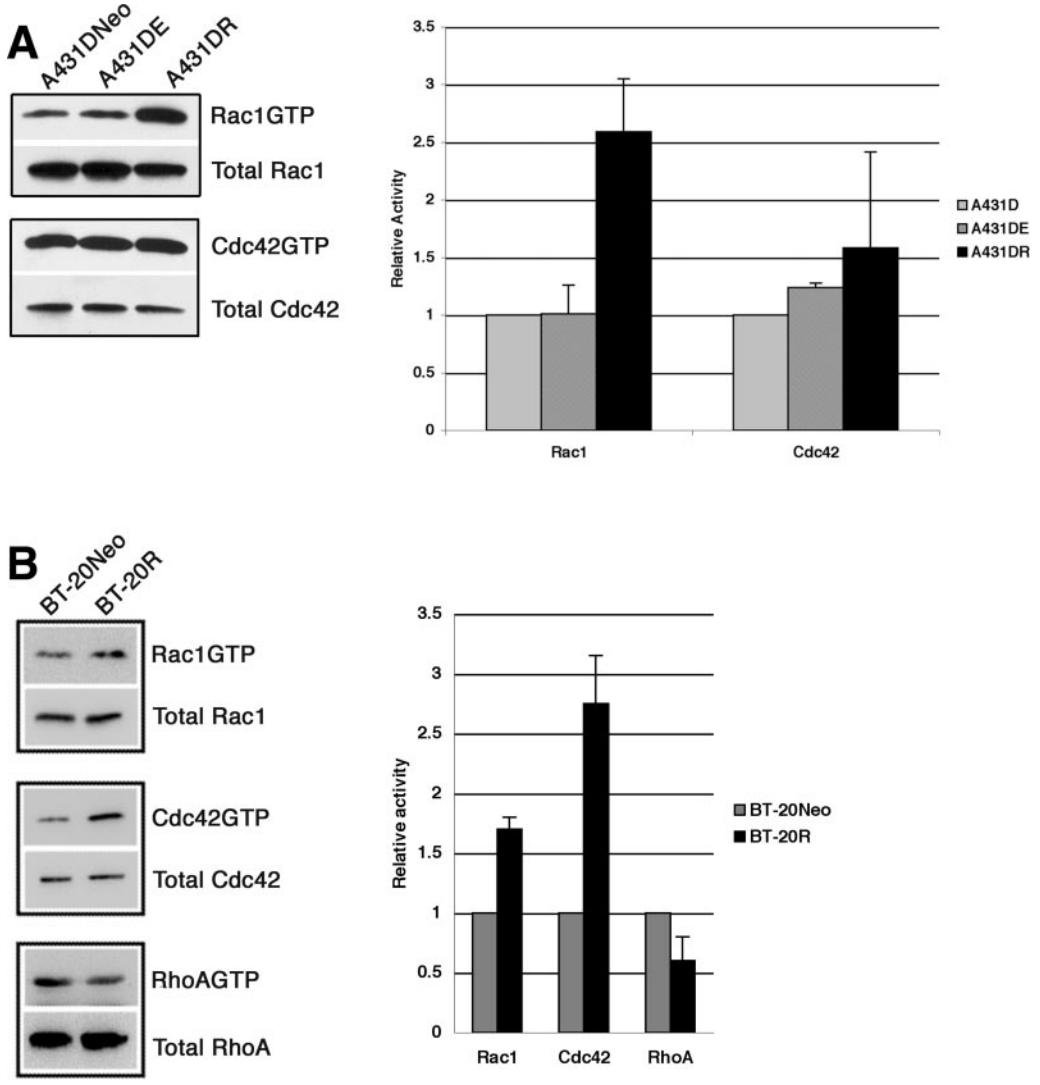

FIG. 5